Catena 208 (2022) 105730

Contents lists available at ScienceDirect

Catena

journal homepage: www.elsevier.com/locate/catena

A holistic methodology to study geochemical and geomorphological control of the distribution of potentially toxic elements in soil

C. Boente [a,b,*], D. Baragaño [c], N. García-González [c], R. Forján [c], A. Colina [c], J.R. Gallego [c]

[a] CIQSO-Center for Research in Sustainable Chemistry, Associate Unit CSIC-University of Huelva "Atmospheric Pollution", Campus El Carmen s/n, Huelva 21071, Spain
[b] Department of Mining, Mechanic, Energetic and Construction Engineering, ETSI, University of Huelva, Huelva 21071, Spain
[c] Environmental Biogeochemistry & Raw Materials Group and INDUROT, Campus de Mieres, University of Oviedo, C/Gonzalo Gutiérrez Quirós. S/N, Mieres 33600, Spain

ARTICLE INFO

Keywords:
Soil pollution
Geomorphology
Potentially toxic elements
Multivariate statistics
Pollution indices

ABSTRACT

Control of Potentially Toxic Elements (PTEs) in soil-polluted areas is needed to address the potential risk that pollution poses to public health and the environment. This study describes an innovative holistic methodology to assess the distribution of PTEs. It is based on the application of multi-variate statistical and geostatistical algorithms, soil pollution indices and geochemical & geomorphological/climate variables (element concentration, watercourses, winds, slope, orientation and visibility). The methodology proposed is exemplified through a comprehensive soil sampling in an area surrounding a former As-Hg mine that presents several sources of pollutants (abandoned mining spoil heaps, metallurgical waste, old chimneys, etc.). Factor analysis identified four main pollutants of concern: Hg, As, Pb and Sb. The mobility of the most abundant PTEs, especially As, and, to a minor extent, Hg, showed a clear influence of climatic/geomorphological variables. Moreover, the pollution indices confirmed that although the soils in the areas around the spoil heaps contain higher concentrations of the pollutants, the influence of the chimneys is present in the whole study area and depends on factors such as orientation and visibility. In contrast, the fingerprint of the spoil heaps showed a PTE distribution more associated with the slope factor and the presence of watercourses eroding the heaps. All things considered, the methodology proposed revealed PTE sources and distribution in a highly complex site and may therefore find application in similar scenarios of contamination.

1. Introduction

Careless mining and industrial practices in the past now pose a risk to the environment and public health. Furthermore, the abandonment of facilities devoted to these sectors without a scrupulous closure plan has led to inappropriate disposal of waste (Hudson-Edwards, 2016). One of the most common problems caused by the mining and industry sectors is the release of Potentially Toxic Elements (PTEs) into environmental compartments, such as soils, water bodies or sediments (Qiao et al., 2020; Hooda, 2010). When PTEs exceed certain thresholds, they are particularly hazardous for soils due to their toxicity, long residence time and the ease with which they are taken up by soil organisms (Kabata-Pendias, 2011). In this regard, the fate of PTEs in the soil environment is dependent on both soil properties and environmental factors (Bolan et al., 2014 and references therein) that control, together with the specific properties of each PTE, their mobility. Mobility is often also related with (bio)availability (the fraction of the total chemical that can interact with a biological target, as defined by Vangronsveld and Cunningham, 1998), and subsequently an increase of (bio)availability is linked to health and environmental issues caused by PTEs as widely reported worldwide (Khanam et al., 2020; Xie et al., 2020; McIlwaine et al., 2017).

Assessment of the geochemical behaviour and spatial distribution of PTEs in soils is a complex process as the following are often involved: multi-element pollution, when the contamination includes more than one PTE (Rate, 2018); multipoint pollution, when there are multiple foci of pollutant dispersal such as chimney emissions, direct dumps, leachates, etc. (Schaefer and Einax, 2016); and external agents, when geographical, meteorological or geomorphological variables (terrain verticality, presence of streams, winds, etc.) play a key role in the

* Corresponding author at: CIQSO-Center for Research in Sustainable Chemistry, Associate Unit CSIC-University of Huelva "Atmospheric Pollution", Campus El Carmen s/n, Huelva 21071, Spain.
E-mail address: carlos.boente@dimme.uhu.es (C. Boente).

https://doi.org/10.1016/j.catena.2021.105730
Received 30 October 2020; Received in revised form 3 September 2021; Accepted 9 September 2021
Available online 16 September 2021

transport of the contaminants (Lieberman et al., 2020; Gallini et al., 2018; Camarero, 2017). In this respect, geochemists and environmental scientists pursue solutions through the use of mathematical tools able to address these issues (Opekunova et al., 2020; Dołęgowska and Michalik, 2019; Tapia et al., 2019; Paiu et al., 2017).

Multivariate statistics are key tools in soil geochemistry studies. They show high capacity to control the variability of geochemical data and to unravel results for multifactor identification (Facchinelli et al., 2001). Among the techniques applied in the study of soil pollution, the Hierarchical Cluster Analysis (HCA) is frequently used to classify samples into groups that share geochemical features (Sierra et al., 2014). A second commonly used tool is Factor Analysis, especially for the identification of pollution sources, as well as for the determination of natural vs. anthropogenic contributions (Hernández-Pellón et al., 2018). Other alternative approaches involve the use of more complex mathematical algorithms, such as Random Forest (Yu et al., 2016) and Bayesian networks (Albuquerque et al., 2017).

Single component geochemical maps have proved useful to report the spatial variation of element concentrations. These maps are used to perform mineral exploration studies (Schnitzler et al., 2019) and soil quality assessments (Jin and Lv, 2020), among other applications. They have been used in the USA (Woodruff et al., 2015), China (Xie et al., 2012) and Europe (Lado et al., 2008). By applying geostatistical models (e.g. kriging) that predicts the spatial distribution of the pollutants (Goovaerts, 1999), these maps provide intuitive solutions. Furthermore, single component maps offer the possibility to combine and compare regionalised variables that differ in nature but that are part of the same environmental problem (McBratney et al., 2003). Notwithstanding, geochemical data can be considered compositional data if the different elements forming a subcomposition are expressed proportionally (Pawlowsky-Glahn and Egozcue, 2006; Tolosana-Delgado et al., 2019). As a consequence, it is possible to transform geochemical data in compositional data to build geochemical maps which represent such elements in proportions (McKinley et al., 2016). This methodology is being gradually more applied in exploratory geochemistry (Braga and Braga, 2020; Sahoo et al., 2020) and in environmental studies (Boente et al., 2018; Petrik et al., 2018), as its firm validity for geochemical data has been demonstrated.

Returning to regionalised variables, these are not restricted to the concentrations of chemical elements. For example, pollution indices can also be calculated to evaluate the degree of soil contamination by PTEs point by point, and afterwards be interpolated to build pollution maps (Pobi et al., 2020; Santos-Francés et al., 2017). These indices, such as Enrichment Factors (Loska et al., 2004) or the Geoaccumulation Index (Teixeira et al., 2019), commonly consider one element. However, there are other valuable indices for those areas affected by multi-element pollution (Wang et al., 2020; Martínez-Guijarro et al., 2019).

Finally, the influence of the external agents previously mentioned can be deduced from the use of all these tools. In this context, additional information can be provided by remote sensing technologies (Florinsky, 1998). Thus, the link between soil pollution and slope, orientation, or visibility of the pollution source can be obtained from Digital Terrain Models (DTMs) constructed by satellite images or by Light Detection and Ranging (LiDAR) devices (Beucher et al., 2017; Vinten et al., 2017; Thomas et al., 2016).

Overall, the main scope of this work is to propose a holistic methodology to assess the mobility of PTEs (multi-element pollution) in soils. The strategy followed combines the use of tools previously described, namely multivariate statistics, geostatistics, pollution indices and the influence of geomorphological variables, to provide a novel approach. To exemplify this approach, the surroundings of La Soterraña, an old Hg mine, were chosen. The soils in this area have been widely studied (Matanzas et al., 2017; Larios et al., 2012; Loredo et al., 2006). They present a notable level of pollution, mainly attributable to highly toxic contaminants (Hg and As), and the features of pollution sources are well described (Fernández et al., 2020). The sharp relief of the study area, together with the presence of several potential mechanisms of pollutant transport, also contribute to the interest of the site as a paradigmatic case in which to apply the novel methodology proposed herein.

2. Materials and methods

2.1. Description of study area and identification of pollution sources

In brief, the facilities of La Soterraña in Lena (Asturias, NW Spain, Fig. 1) were used for the underground exploitation of Hg and the pyrometallurgical processing of the ores from this mine and others in the area (Loredo et al., 2006). The ores exploited were cinnabar (HgS), orpiment (As_2S_3), realgar/pararealgar (AsS) and arsenopyrite (FeAsS), originated in a low-temperature hydrothermal process that took place in fractured limestones, lutites and sandstones (Loredo et al., 1988). Additional information about the geomorphology, vegetation and climatic conditions of the site can be found in Matanzas et al., 2017 and references therein.

The pollution in La Soterraña (650 m.a.s.l.) and its surroundings is attributable mainly to two sources (Fig. 1). The first consists of two spoil heaps of mine waste that was indiscriminately dumped and additional minor accumulations of extremely toxic metallurgical waste (see Fernández et al., 2020 for details); this waste has a high content of sulphide/oxide minerals that are susceptible to react with water and/or air. The second source corresponds to several chimneys (up to 13 m high), located uphill of the study area, and that released gases from the pyrometallurgical plant daily between 1950 and 1974.

2.2. Sampling design, collection and preparation

The main pollution sources were located approximately at the centre of the study area, (Fig. 1). The sampling campaign is shown in Fig. 1. First, a 1 km-radius from the centroid of La Soterraña site was delimited for the sampling. We collected 92 soil samples from grasslands within the circle and outside the contour of the site. The samples were collected in a random fashion. However, certain areas were inaccessible due to the challenging topography and dense vegetation and therefore were not sampled.

Each sample is composed of five subsamples taken from each vertex of a 1-m edge square and its central point. Samples were collected using a stainless steel tool and then stored in plastic bags and transported to a laboratory, where they were air-dried to prevent the vaporisation of Hg. Afterwards, they were passed through a 2-mm mesh screen and the particles below 2 mm diameter were quartered by means of a Jones riffle splitter in order to homogenise the soil. Samples were finally ground at 400 RPM for 40 s in a RS100 Retsch mill, obtaining particles sizes of $<$100 μm.

2.3. Chemical analysis

1-g representative sub-samples were sent to Actlabs (ISO-9002 and ISO-17025 accredited laboratory in Vancouver, Canada) and analysed by means of ICP-MS (Inductively Coupled Plasma - Mass Spectrometry) after aqua regia digestion, to determine the total concentration of the following 35 elements (detection limits shown in parentheses): Ag (0.1 ppm); Al (0.01%); As (0.5 ppm); Au (0.5 ppb); B (20 ppm); Ba (0.5 ppm); Bi (0.1 ppm); Ca (0.01%); Cd (0.1 ppm); Co (0.1 ppm); Cr (1 ppm); Cu (0.2 ppm); Fe (0.01%); Ga (1 ppm); K (0.01%); La (1 ppm); Mg (0.01%); Mn (1 ppm); Mo (0.1 ppm); Na (0.001%); Ni (0.1 ppm); P (0.001%); Pb (0.1 ppm); S (1%); Sb (0.1 ppm); Sc (0.1 ppm); Se (0.5 ppm); Sr (1 ppm); Te (0.2 ppm); Th (0.1 ppm); Ti (0.001 ppm); Tl (0.1 ppm); V (2 ppm); W (0.1 ppm); and Zn (1 ppm). Hg (0.01 ppm) was analysed by cold-vapour FIMS (Flow Injection Mercury System). Samples were analysed using strict quality controls, using five blanks, five duplicates, and ten analyses of standard reference materials (internal standards and OREAS45EA), which were inserted into the sample sequences, thereby providing a

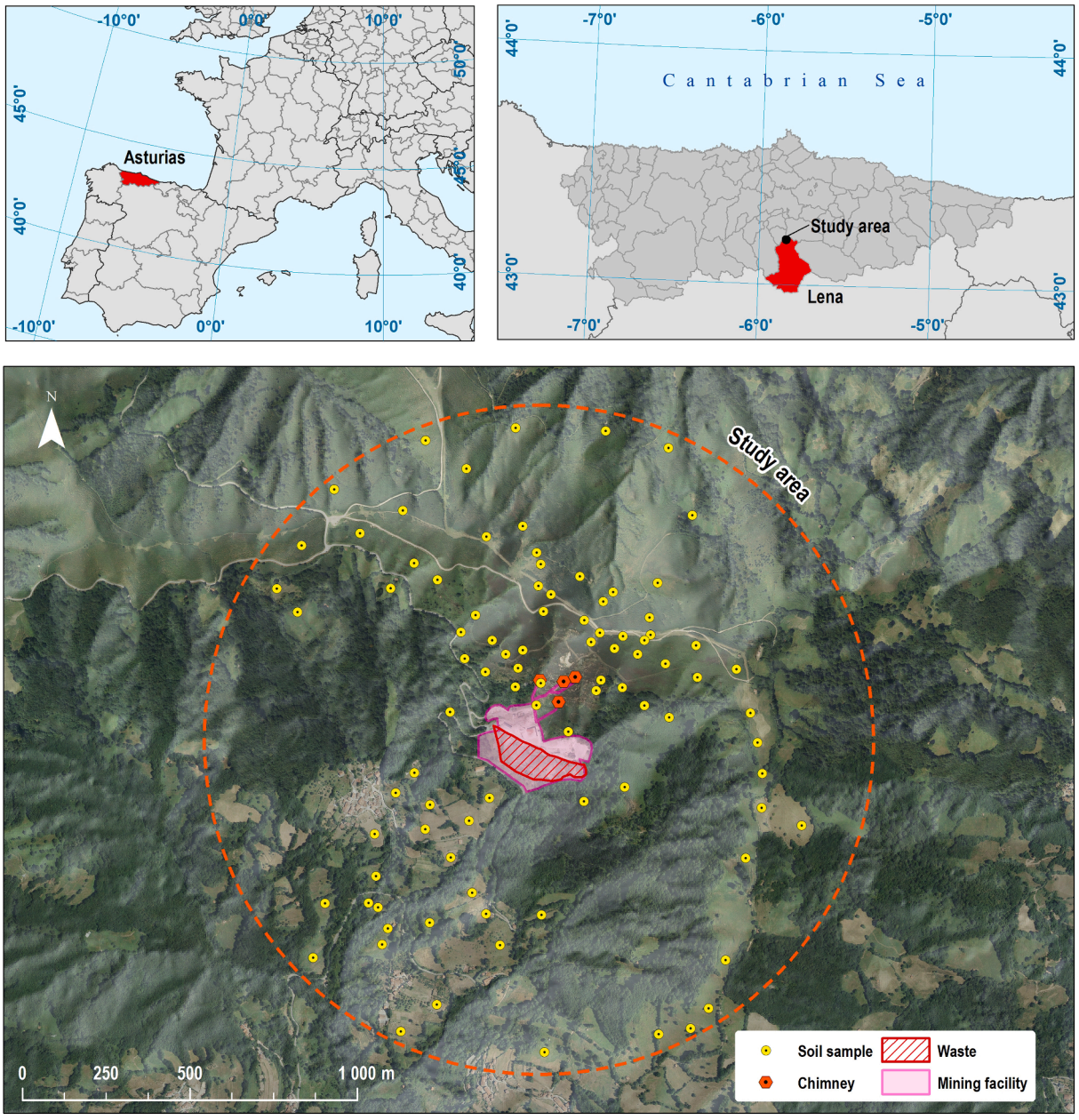

Fig. 1. Location of the 1-km circumference study area in Asturias, NW Spain (43°11′34′′ N, 5°50′36′′ W) and location of soil samples, facilities and foci of pollution.

measure of background noise, accuracy and precision. The mean Relative Standard Deviation (RSD) for the trace elements analysed in the duplicates ranged between 0 and 2.1 ppm, except for Cu (4.91 ppm) and Mn (9.89 ppm). In the case of major elements, Fe (0.028%) and Al (0.024%) presented the higher values, while the rest showed RSD below 0.01%.

2.4. Univariate and multivariate statistics

Univariate statistical parameters were calculated for all the PTEs analysed to obtain a preliminary perspective of the extent of pollution. Additionally, elements were compared with their corresponding Risk-Based Soil Screening Levels (RBSSLs) for Asturias (BOPA, 2014), which set the official pollution limits.

Factor Analysis through Principal Component Analysis (PCA) allowed grouping of the elements in terms of their nature or anthropogenic associations (Borůvka et al., 2005). The factor extraction was determined by the Kaiser/Gutmann criterion with varimax rotation to facilitate the interpretation of the factors by making each variable having either large or small contributions to each factor, as suggested for geochemical data (Reimann and De Caritat, 2005). Additionally, a Hierarchical Cluster Analysis (HCA) was applied to classify the samples. This was done using Ward's algorithm and the Squared Euclidean distance, maximising the variance between groups and minimising it between members of the same group. All the statistical analyses were performed using SPSS V.24 software (IBM Corp., 2016).

2.5. Cartographic tools and geostatistics

The influence of variables linked to geomorphological or geographic features on pollutant dispersal was also studied. In this regard, slope, orientation and visibility of pollution sources were considered. The representations of these variables were generated in ArcGIS v-10.2.2 (Esri Inc, 2014), over the basis of a Digital Terrain Model (DTM) provided by the Spanish Instituto Geográfico Nacional (IGN) with a mesh resolution of 5 m. The results were integrated with the cluster

distribution addressed in Section 2.3.

Additionally, the spatial distributions of the main pollutants, namely As and Hg, as well as other associated PTEs of concern (Sb and Pb), were interpolated by means of Ordinary Kriging (OK) after log-transformation to improve the normality of data (Webster and Oliver, 2007). When computing the semivariograms, it was decided to assume spatial isotropy since the search for preferential directions is one of the focus of the study. All modelled semivariograms and interpolations were carried out through the official *Geostatistical Wizard* module in ArcGIS v-10.2.2 (Esri Inc, 2014).

Moreover, a centred-log ratio (clr) transformation (Aitchison, 1986) was also applied to a sub-composition with PTEs, as the inclusion of major elements (e.g. Al, Fe, Ca, etc.) "dilute" the concentrations of trace elements. Thus, this sub-composition, together with Hg and As, included: Ag, Ba, Bi, Cd, Co, Cr, Cu, Ga, La, Mo, Ni, Pb, Sb, Sc, Sr, Te, Th, Tl, V W and Zn. For the transformation, the software CodaPack (Comas-Cufí and Thió-Henestrosa, 2011) was used. Geostatistical maps for Hg, As, Pb and Sb were built through Ordinary Kriging too in order to offer comparable results.

2.6. Soil pollution indices and geochemical ratios

Two integrated indices were used to evaluate the information collected. These two indices were calculated for the two main pollutants (As and Hg):

(i) The Modified Pollution Index (MPI)

Defined by Brady et al. in 2015, this index was originally used to determine pollution by heavy metals in sediments (Eq. (1)):

$$MPI = \sqrt{\frac{(EF_{average})^2 + (EF_{max})^2}{2}} \quad (1)$$

where $EF_{average}$ is the average Enrichment Factor (EF) for the whole set of PTEs in the soil considered, and EF_{max} is the maximum value of the EF for a single element in the soil. In his work, Brady defined 6 classes for his MPI index: MPI < 1, Unpolluted; 1 < MPI < 2, Slightly polluted; 2 < MPI < 3 Moderately Polluted; 3 < MPI < 5, Moderately polluted-heavily polluted; 5 < MPI < 10, Heavily polluted; and 10 < MPI, Severely polluted.

Note that the EF is calculated through Eq. (2):

$$EF_{j,S} = \frac{\left[\frac{C_j}{C_{ie}}\right]_S}{\left[\frac{C_j}{C_{ie}}\right]_{RB}} \quad (2)$$

where C_j is the concentration of element "j" (As or Hg) in sample "S" and in the selected reference background (RB), and C_{ie} is the concentration of V, a lithogenic conservative element that is resistant to chemical weathering (see Boente et al., 2020 and references therein). RB values were taken from the official dataset used for determining the RBSSLs in the region of Asturias (Fernández et al., 2018); i.e. As (39.21 mg/kg), Hg (0.49 mg/kg) and V (47.43 mg/kg).

(ii) The Soil Pollution Index (SPI)

This variable was first defined in Boente et al. (2017). It measures the degree of soil pollution at a given point in terms of the legal limits of pollution established:

$$SPI = \frac{\sum \frac{C_j}{RBSSL_j}}{N} \quad (3)$$

where Cj is the concentration of element j (As or Hg), RBSSLj is the soil screening level of element j, and N is the number of pollutants considered (in this study N = 2; As and Hg).

Both the MPI and SPI are regionalised variables and were determined for each of the sampling points. Thus, they were interpolated by means of OK. On the other hand, geochemical ratios were determined using the concentrations of As, Hg and V, in order to compare the geochemical fingerprint between the groups obtained by the HCA. Furthermore, these ratios were contrasted with the SPIs described above.

3. Results and discussion

3.1. Soil pollution overview

Previous studies of La Soterraña identified two main sources of pollution in the site (Loredo et al., 2006; Matanzas et al., 2017): i) mining waste, a dark residue from distilled Hg ore which had been dumped in two spoil heaps across the plot; and ii) metallurgical waste, mainly flue dust that emanated from five chimneys inside the facility, dispersing dust and gasses to the surrounding soils. According to recent analyses, the mining waste contains averages of 23,000 mg/kg of As and 6000 mg/kg of Hg, while the flue dust has 138,200 mg/kg of As and 33,000 mg/kg of Hg (Fernández et al., 2020). Moreover, As in the flue dust presents notable bioavailability (14.8%), with the aggravating circumstances of fine grain-sizes and a significant proportion (64.6%) of As (III) (see Fernández et al., 2020 for details).

Topographic results from the DTM representation are shown in Fig. 2. This representation allows initial prediction of areas affected by the different transport mechanisms (air or water). Thus, the facilities of La Soterraña, and therefore the chimneys and spoil heaps, are located amid several valleys on the southern side of a mountain, which would be the area most susceptible to pollution. However, sample collection also covered the northern slope and the water divide. The same figure shows surface runoff. In fact, some streams cross the facilities and wash the waste present, thereby potentially transporting pollutants to the valley below. However, these mountain watercourses are active only during certain parts of rainy seasons or snowmelt periods.

The results of the multi-element analysis of the 92 soil samples are shown in Table 1. A high Relative Standard Deviation (RSD) coefficient usually reveals the absence of normality conditions in the distribution and it is a handicap for geostatistical representation. In this case a high RSD was found not only for As and Hg, but also for Ba, Ca, Na and Sb. Differences in Ca or Na are explained by the geology of the area (Loredo et al., 1988), while the presence of Ba and especially Sb is related to As in the geochemistry of the ores (Gallego et al., 2015). The remaining elements, including some rare earths or other PTEs, showed stable concentrations with low RSDs.

The maximum concentrations of Hg and As were two or up to almost three orders of magnitude above the RBSSLs. Other elements that surpassed the legal limits at least once were Ba, Pb, Sb and V. However, Hg and As were the only elements whose mean concentration notably exceeded the limits (more than one order of magnitude).

To determine the relevance of these Hg and As concentrations, a potential geochemical threshold specific for the area was calculated through the means of As and Hg contents, respectively, plus two times the standard deviation of the data set; after excluding the main outliers (eight samples corresponding to percentile 90 of the Mahalanobis distance) (Meeker et al., 2017). The resulting values for the 3.14 km^2 under study were 631 $mg{\cdot}kg^{-1}$ for As and 51 $mg{\cdot}kg^{-1}$ for Hg. These values were markedly above any international backgrounds or thresholds, and specifically those of Asturias (39.21 $mg{\cdot}kg^{-1}$ for As and 0.39 $mg{\cdot}kg^{-1}$ for Hg (Fernández et al., 2018) and the neighbouring region of Cantabria (46.18 $mg{\cdot}kg^{-1}$ for As and 0.21 $mg{\cdot}kg^{-1}$ for Hg (Boente et al., 2020), both calculated by the same methodology used here (mean plus two times standard deviation).

The spatial distribution of As and Hg, in addition to others that occasionally surpassed RBSSLs (Sb and Pb), was geostatistically mapped through OK (Fig. 3). The experimental variograms for log-transformed

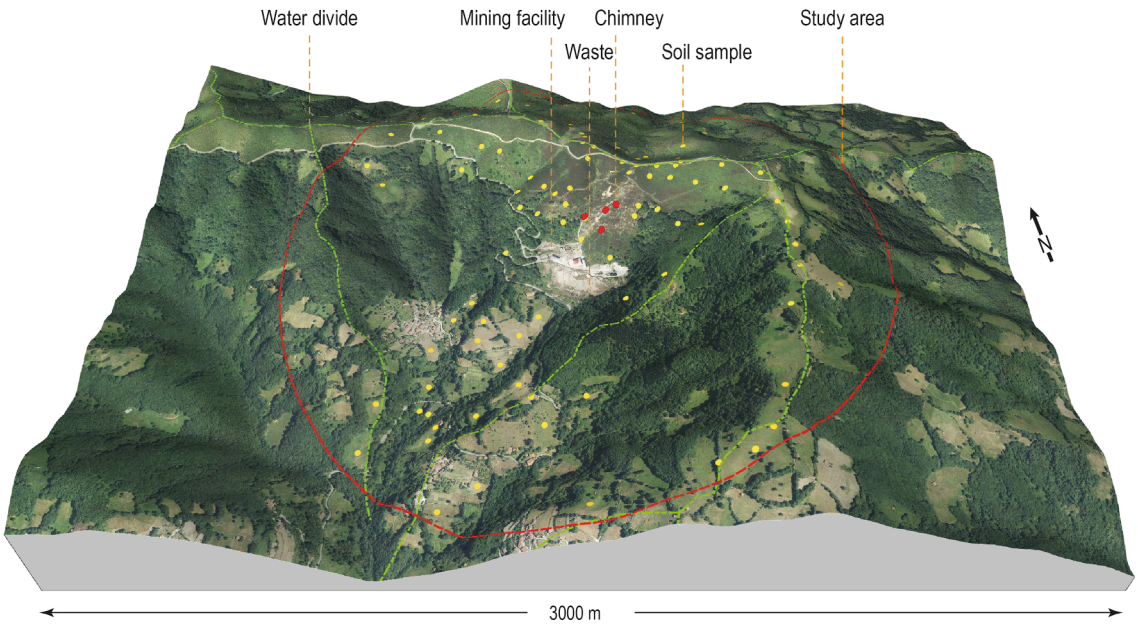

Fig. 2. Three-dimensional view of the study area, with the topographic level and the main surface runoffs and water divides. Pollution sources and sampling points are included.

Table 1
Descriptive statistics for the analysis of 92 soil samples from La Soterraña surroundings and RBSSLs (BOPA, 2014) for Asturias. All units are expressed in mg·kg^{-1}, except RSD, which is expressed in %. In bold, PTEs whose mean concentration is notably higher than the RBSSL.

Element	RBSSL	Minimum	Maximum	Mean	Median	SD	RSD
Hg	**1**	**0.6**	**860**	**46**	**17**	**138**	**298**
As	**40**	**22**	**9920**	**429**	**165**	**1086**	**253**
Ag	2	0.1	0.2	0.1	0.1	0.02	20
Al (%)	–	0.9	5.0	1.8	1.6	0.7	40
Ba	1540	55	3370	151	110	341	225
Bi	–	0.1	0.5	0.3	0.3	0.1	20
Ca (%)	–	0.02	23	0.6	0.2	2.5	397
Cd	2	0.1	1.5	0.4	0.3	0.2	64
Co	25	1.0	22	11	12	4.6	43
Cr	10,000	14	63	27	25	10	35
Cu	55	5.8	85	22	21	12	57
Fe (%)	–	0.7	6.5	3.2	3.2	0.7	22
K (%)	–	0.1	1.0	0.3	0.2	0.1	47
La	–	7	30	14	13	4.5	32
Mg (%)	–	0.03	0.45	0.1	0.1	0.1	71
Mn	2135	31	2070	554	549	320	58
Mo	6	0.4	3.6	0.8	0.8	0.4	45
Na (%)	–	0.01	1.3	0.04	0.02	0.1	363
Ni	65	4.2	55	23	23	11	49
Pb	70	22	111	42	38	15	36
Sb	5	0.2	44	1.7	0.8	4.7	280
Sc	–	1.0	10.3	3.7	3.4	1.8	48
Sr	–	16	786	87	50	110	127
Th	–	1.4	9	3.7	3.3	1.8	48
Ti (%)	–	0.001	0.02	0.002	0.001	0.002	111
Tl	1	0.1	0.7	0.2	0.2	0.1	46
V	50	20	92	42	40	14	33
W	–	0.1	0.9	0.1	0.1	0.1	77
Zn	455	26	228	96	94	39	41

data (Fig. 4) showed coherent curves, with a nugget effect below 30%, even for those elements with the highest spatial variability over shorter range values (As and Hg). These values are acceptable for an OK interpolation. Both logarithmic and clr transformations enable dealing with extreme values so, subsequently, none of them was removed.

With regard to Hg and As (Fig. 3a, 3b), although they showed similar distributions, there were noteworthy differences. For instance, As was more present around the chimneys. This observation is coherent with the fact that Hg was recovered mostly by condensation during the pyrometallurgical process (Fernández et al., 2020), whereas As, with a higher boiling point, was incorporated mainly into flue dust and therefore larger amounts of this PTE were dispersed through the chimneys than Hg.

However, Hg (Fig. 3b) showed a lower mobility in this case and was more intensely distributed across the plot, specifically around the two main foci (chimneys and heaps). Areas below the spoil heaps were more affected, thereby evidencing that the washing by surface runoff and wind erosion of the heaps contribute to the dispersion of Hg. For this

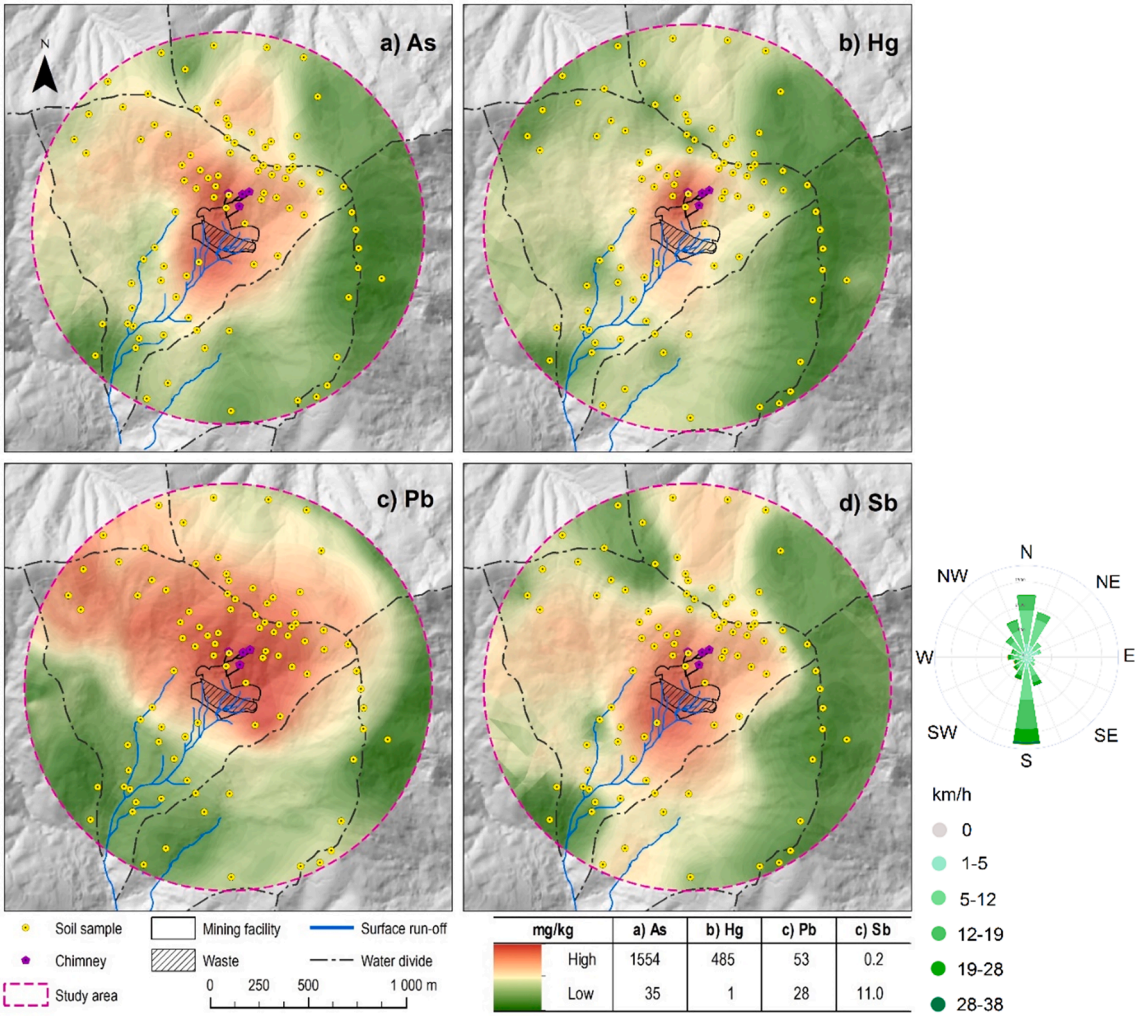

Fig. 3. Distribution of As, Hg, Pb and Sb obtained by ordinary kriging and wind rose corresponding the last 30 years (Meteoblue, 2021).

reason, Hg tended also to reach the valley downstream. These visual interpretations are checked analytically in following sections.

Pb presented a regular distribution, oscillating in stable ranges of between 28 and 53 mg·kg^{-1}, revealing that the extreme values in Table 1 correspond to punctual disposals and that this element does not present other dispersion mechanisms. Finally, Sb showed a fingerprint that was practically equal to that of As. This observation is coherent with the fact that As and Sb are metalloids that are well correlated (Okkenhaug et al., 2012) and tend to move together, and moreover, with respect to their mobility, the eastern sector of the study area appeared to be the least affected.

PTEs distribution may be explained attending wind patterns since, according to data from MERRA-2 (Modern-Era Retrospective Analysis from NASA, Gelaro et al., 2017), winds in the study area (in the last 30 years) are preferentially northerly from mid-April to mid-September, southerly from mid-September to mid-March, and westerly from mid-March to mid-April, thus coinciding with the wind directions shown in Fig. 3 (Meteoblue, 2021). It must be pointed out that a better approach would require local and specific wind measures taken in the decades (1950s–1970s) of maximum activity in the mining-metallurgy area (Loredo et al., 2006); unfortunately, there is no wind data available from that period in the study area.

Finally, geostatistical interpolations and maps were done for clr-transformed data (Supplementary Material, Fig. SM1). Note that compositional data represents relative enrichments and, consequently, it seems coherent that the distributions of Hg and As in Fig SM1 are similar in Fig. 3, since, as previously mentioned, they showed extreme concentrations in the areas highlighted in Fig. 3 and, therefore, their relative enrichment is higher (as showed in Fig SM1). The same fact can be applied for Sb, as it is included in the mineral paragenesis of the ore deposit (Loredo et al., 2006). Nevertheless, Pb shows a different map (Fig. 3c and Fig SM1.c) with a relative enrichment in the central parts and high enrichments in areas where the previous PTEs are not excessively enriched. This occurs due to the fact that extreme concentrations of an element (e.g. 1554 ppm of As or 485 ppm of Hg within the mining facility) overshadow concentrations of elements that are mainly part of the background and show a more regular distributions; i.e., the proportions of non-pollutants will be higher in areas where the concentration of pollutants (As, Hg) is lower. As a conclusion, compositional data analysis is a suitable tool to discriminate pollutants from non-pollutants attending to the relative enrichment.

3.2. *Multivariate study: Geographical clustering*

The next stage of the analysis addressed the associations between elements. A factor analysis was carried out (PCA and varimax rotation) for the multi-element data after a logarithmic transformation of the dataset to improve the normality conditions. The results (Table 2) are robust and reliable, as shown by a score 0.804 for the Kaiser-Meyer-Olkin (KMO) measure of sampling adequacy, the high communalities, and 85% of the total variance explained by the factorial solution obtained (Kaiser, 1974).

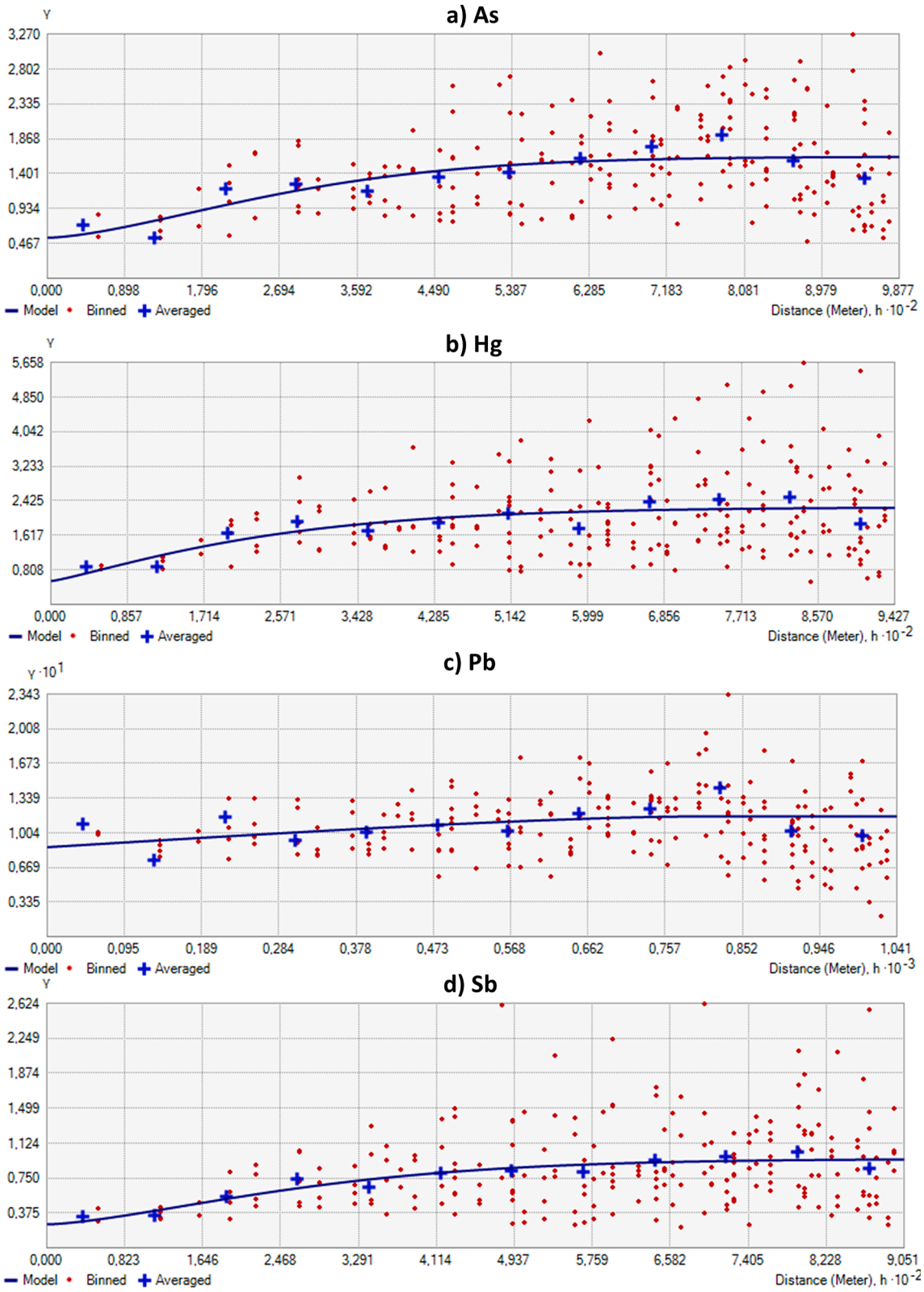

Fig. 4. Semivariograms obtained for the Ordinary Kriging geostatistical analysis.

Factor 1 (F1) presented mainly natural-sourced elements, probably related to Fe-Al oxides that are common in the area and lithogenic elements such as V, the conservative element used for calculating the MPI. Factor loadings in F2 were led by PTEs present at low concentrations in the area (Co, Ni, Zn or Cu) and that are usually linked to carbonated rocks with high content of Mg in the Cantabrian Mountains (Boente et al., 2020). F3 showed high loads for Na, Ba, K, all alkali elements associated with feldspars and clays, without PTEs, thereby suggesting a natural source. In contrast, F4 revealed a quartet of the main pollutants (Table 2, Fig. 3): Hg, As, Sb and Pb. Finally, F5 was limited to Cd.

To gain a better understanding of similar geochemical profiles, we performed an HCA, and, in general terms, geography clearly influenced

Table 2
For all the sampling dataset: Factor loadings, percentage of variance explained by the Varimax-rotated factors, extracted by principal components and communalities.

	F1	F2	F3	F4	F5	Com.
V	**0.892**	−0.004	−0.075	0.216	0.333	0.959
Cr	**0.878**	0.237	0.096	0.150	0.288	0.943
La	**0.855**	0.303	−0.004	0.274	−0.147	0.919
Sr	**0.794**	0.083	0.386	0.186	−0.033	0.822
Th	**0.782**	0.388	0.091	−0.048	−0.384	0.921
Fe	**0.643**	0.408	−0.524	−0.003	0.052	0.857
Al	**0.601**	0.297	0.184	0.261	0.506	0.808
Co	0.298	**0.898**	−0.026	−0.103	−0.042	0.909
Ni	0.401	**0.869**	0.116	−0.024	0.064	0.934
Zn	0.211	**0.849**	0.133	0.142	0.301	0.894
Cu	0.076	**0.843**	0.149	0.174	−0.275	0.845
Mn	0.187	**0.784**	0.085	−0.103	0.160	0.693
Mg	−0.170	**0.682**	0.485	0.039	0.170	0.759
Na	−0.039	−0.031	**0.937**	0.134	0.046	0.901
Ba	0.103	0.292	**0.896**	0.150	0.049	0.924
Ca	0.099	0.480	**0.679**	0.144	0.149	0.744
K	0.448	0.382	**0.594**	0.331	0.118	0.822
Mo	0.452	0.011	**0.570**	0.128	0.324	0.650
As	0.175	−0.042	0.092	**0.892**	0.241	0.894
Sb	0.155	0.039	0.292	**0.891**	−0.006	0.906
Hg	0.174	0.124	0.156	**0.888**	−0.061	0.863
Pb	0.126	−0.141	−0.013	**0.732**	0.497	0.819
Cd	0.075	0.236	0.325	0.236	**0.749**	0.784
Exp. Variance (%)	40.491	57.287	71.844	79.212	85.091	

the HCA results (Fig. 5). Cluster 1 (C1) comprised mainly samples taken from the surrounding of La Soterraña site. In contrast, C2 corresponded to those halfway between the facilities and the top of the mountain. C3 presented a wide scattering and predominated mainly across the water divide. C4 corresponded principally to samples collected on the northern face of the mountain. Finally, C5 included most of the samples located beneath the facilities, corresponding to the soils directly affected by the surface runoff crossing the spoil heaps.

3.3. *Integration of geochemical, geomorphological and pollution data*

The HCA provided robust information about different profiles related to the geographical location. In this regard, to ascertain the geochemical differences among them, geochemical ratios were developed (Fig. 5). Comparison of the As/V vs. Hg/V ratios (Fig. 6a) revealed a relatively similar pollution fingerprint for groups C2 and C3, and for C4 and C5, respectively. Regarding the geomorphology of the area, C2 and C3 were in the areas with the lowest slope while the other two were from higher slopes. In turn, the fingerprint of C1, which corresponded to samples nearer the sources of pollution (spoil heaps and chimneys), differed greatly.

The As/Hg relationship (Fig. 6b) revealed that although C2 and C3 showed the same fingerprint using the ratios above, there were some differences between these groups. Samples belonging to C3 were far from the pollution sources and showed the lowest pollutant concentrations (Table 3), which suggests a more important geogenic influence in this group. The pollution indices (see also Table 3) also indicated that samples included in C3 showed the lowest level of pollution (Fig. 5c and 5d).

Having examined the geochemical behaviour of the pollutants, we proceeded to study the interaction of geochemical variables with geographical and geomorphological variables (Table 3).

First, the highest levels of As and Hg pollution found in C1 (the samples nearest to the centre of the site) corresponded mostly to areas with high slopes (20–45°) facing S-SW, which in the north hemisphere

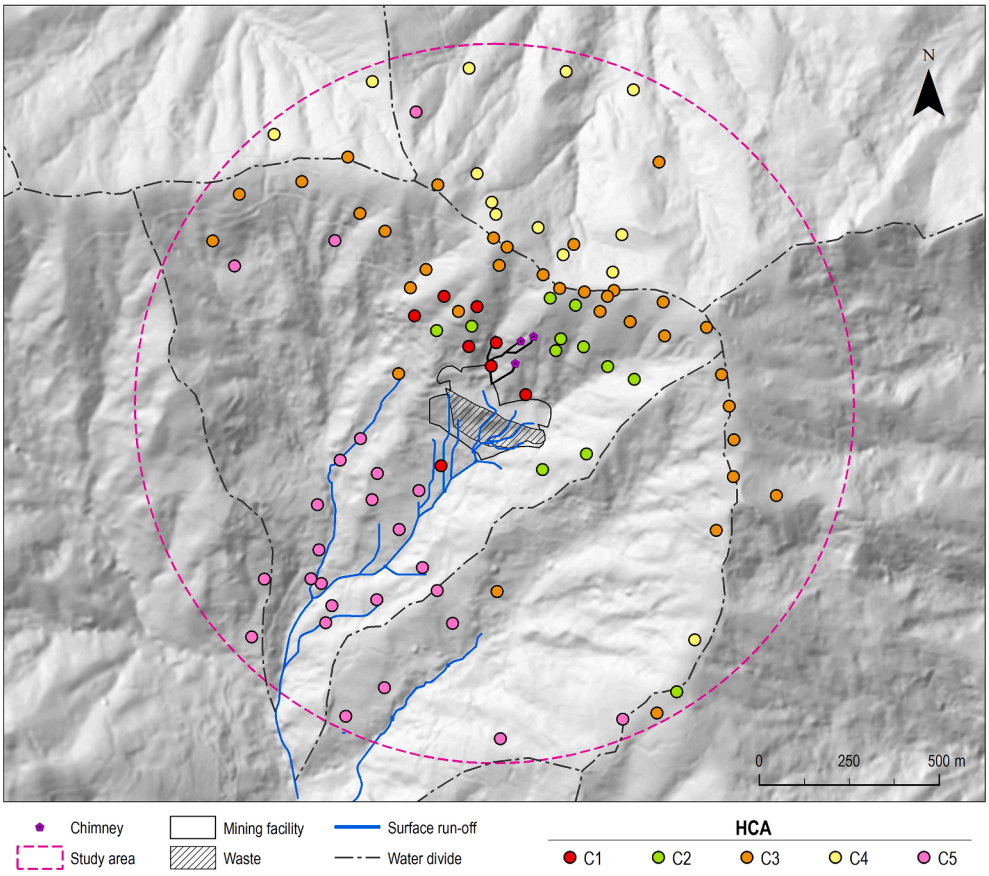

Fig. 5. Graphical representation of the hierarchical cluster analysis.

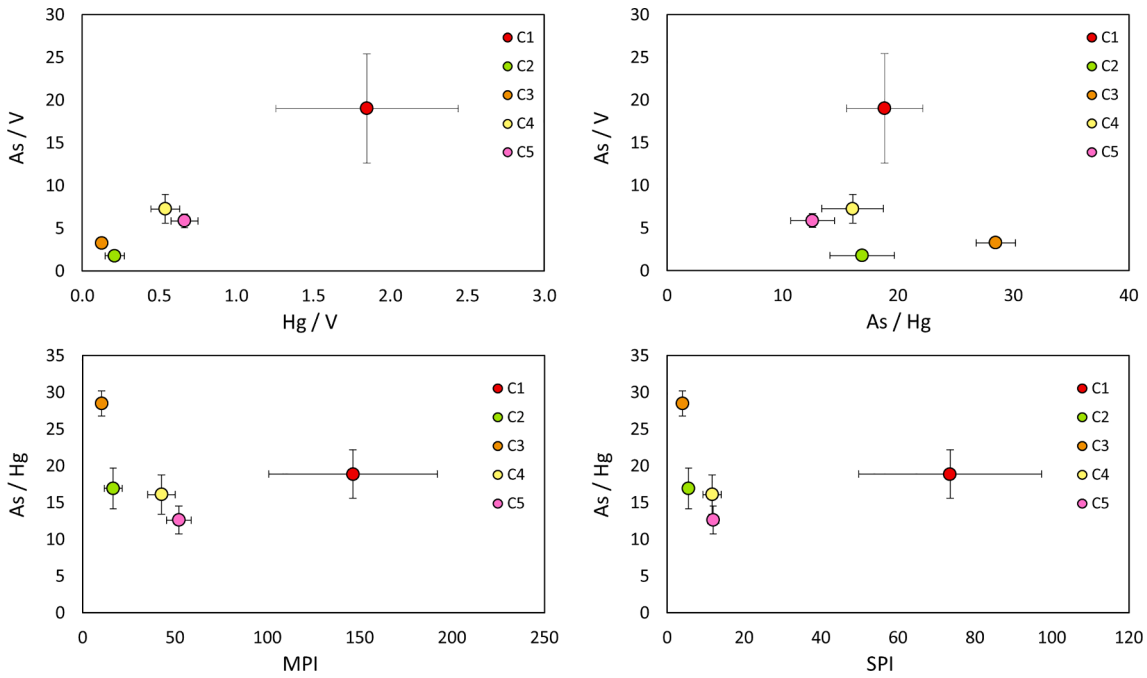

Fig. 6. Geochemical ratios using element concentrations and pollution indices: a) As/V vs. Hg/V; b) As/V vs. As/Hg; c) As/Hg vs. MPI; and d) As/Hg vs. SPI.

Table 3
Pollutant content, and geographical and geomorphological features for each cluster.

			C1	C2	C3	C4	C5
Concentrations	**Hg mean (mg·kg^{-1})**		121	9	5	17	20
	Hg RSD (%)		195	106	82	71	61
	As mean (mg·kg^{-1})		1059	78	126	240	172
	As RSD (%)		173	111	70	92	65
% of samples in terms of the angle of the slope		**Tot. Samples (No.)**	**C1**	**C2**	**C3**	**C4**	**C5**
	0.0° to 10°	**13**	*4*	*20*	*21*	*8*	*23*
	10.1° to 20.0°	**36**	*14*	*53*	*50*	*23*	*64*
	20.1° to 30°	**29**	*43*	*27*	*21*	*62*	*9*
	30.1° to 45°	**14**	*39*	*0*	*7*	*8*	*5*
		Tot. Samples (No)	**C1**	**C2**	**C3**	**C4**	**C5**
% of samples in terms of the orientation of the slope	**N**	**5**	*4*	*0*	*0*	*31*	*0*
	NE	**6**	*0*	*7*	*7*	*31*	*0*
	E	**1**	*0*	*7*	*0*	*0*	*0*
	SE	**7**	*4*	*7*	*7*	*0*	*18*
	S	**29**	*43*	*20*	*36*	*0*	*41*
	SW	**24**	*32*	*27*	*29*	*0*	*32*
	W	**13**	*14*	*27*	*14*	*15*	*5*
	NW	**7**	*4*	*7*	*7*	*23*	*5*
% of samples from chimneys and spoil heaps are visible		**Tot. Samples (No)**	**C1**	**C2**	**C3**	**C4**	**C5**
	Visible	51	*82*	*27*	*50*	*0*	*59*
	Not visible	49	*18*	*73*	*50*	*100*	*41*

implies exposure to sun and therefore Hg vaporisation. Additionally, due to the proximity, the visibility of the site from this area is also high. All these factors favour the displacement of PTEs, and the high concentrations of these pollutants in these soils may affect other areas.

In C2, the concentration of As and Hg was lower, but the RSD was high, thus implying more variability. This is coherent with the greater geographical dispersal of samples in this cluster. Samples belonging to C2 also face mainly SW-W, and unlike C1, the sources (spoil heaps and chimneys) are not visible from the majority of sampling points, and the slope is also less than in C1 (10-20°). This pattern is generally repeated in C3, which presents samples with the lowest concentration of Hg. In fact, this group is geographically dispersed and most samples are those located furthest from the sources, and thus coherent with low Hg mobility.

The samples included in C4 present very stable values (low RSDs), with the third highest content of As and Hg. All the samples in this group are in the northern face of the mountain, from where the facilities are not visible. Therefore, the pollutants may have reached this zone by atmospheric deposition, probably through the chimneys given the preferential wind direction (northerly) in the summer.

Finally, C5, including mainly the samples most affected by surface runoff, was the second group in terms of Hg and As content, also with stable values. Sample in this group were from the area with the lowest slope (87% of soils are below a 20° incline), thereby indicating that downstream plains are polluted in regular proportions.

Finally, in order to provide a global overview, the MPI, constructed through the enrichment factors of Hg and As and its distribution, was represented by means of OK (Fig. 7a). Except for the eastern sector, which was less affected by winds and was far from the facilities, the remaining study area can be considered "severely polluted", as reflected by an MPI score consistently exceeding 10 (Brady et al., 2015). We extracted the contour of the central area (namely, "high pollution contour"); i.e. the most affected zone, and introduced it into the rest of the maps in order to make comparisons (see Fig. 6).

In contrast, the SPI (Fig. 7b) reveals the most polluted areas based on the RBSSLs in force. The results were similar to those of the MPI and thus the complete pollution contour defined above emerges as the most problematic area from a legal perspective. Thus, priority environmental remediation actions should focus on the surroundings of the facilities.

With respect to geomorphology, Fig. 7c, 7d and 7e graphically summarise the relationship between the degree of pollution and the slope of the mountain, its orientation, and visibility of the spoil heap and chimneys, respectively. Regarding the first parameter, areas with a greater slope did not necessarily present a higher degree of pollution, as

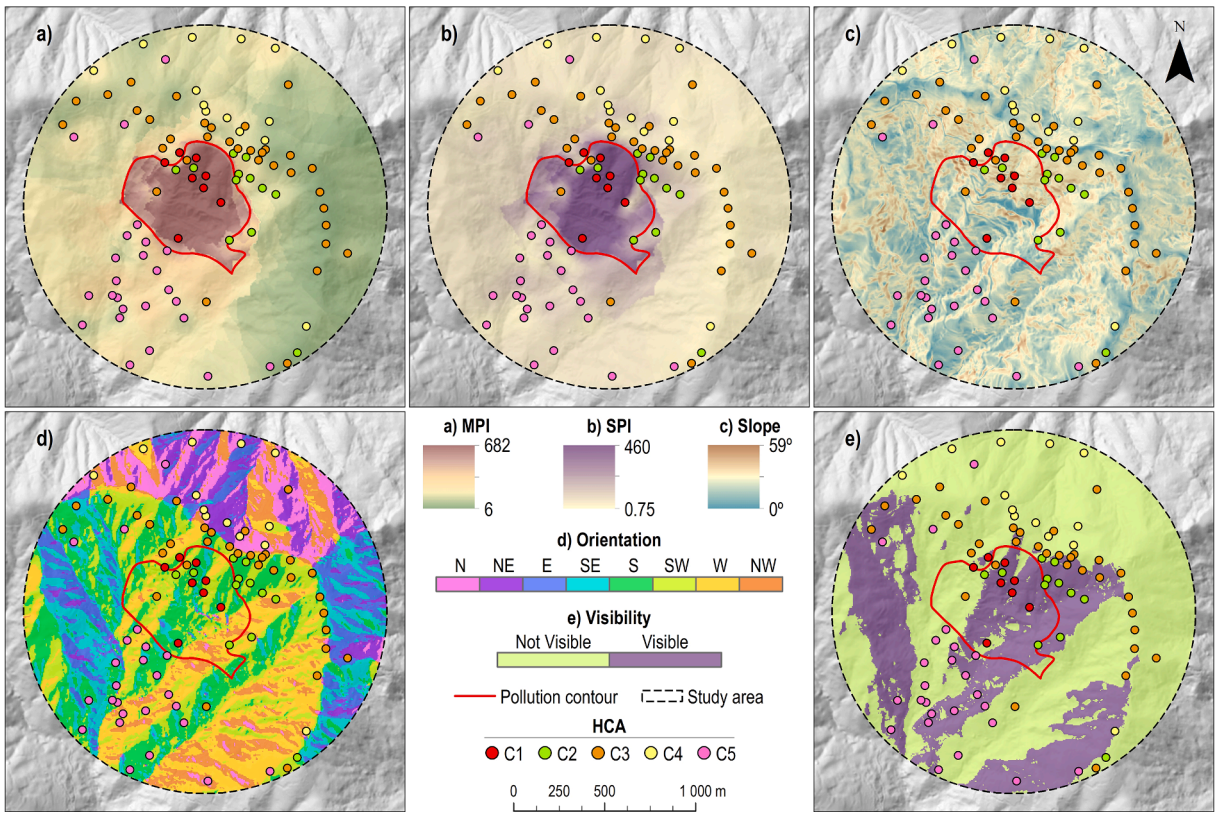

Fig. 7. a) MPI interpolation through OK; b) SPI interpolation through OK; c) Slope of the soil (°); d) Orientation of the soil; e) Visibility of the spoil heaps and chimneys.

slope is highly heterogeneous across the study site, alternating flat areas (0–8° of inclination) and with most soils on a high slope (>15°), thus revealing independence from this parameter. This perspective changes when considering orientation. In this regard, we detected a certain degree of parallelism between the different faces of the mountain and the most polluted contour (predominance of S/SW orientations). For instance, the highest MPI values did not reach those of the north-facing side of the mountain or those of some protected areas orientated to the east. Finally, the visibility study (Fig. 6e) confirmed that the high pollution contour is not fully in the visibility range of the chimneys or the spoil heap.

On the basis of our observations, we can infer the following: 1) The closer to the spoil heaps, the higher the presence of extremely high concentrations of PTEs. In this sense, surface runoff favours the dispersion of the PTEs to valleys downstream, whose low slope favours the permanence of the pollutants; and 2) The chimneys are the main source of pollution for the rest of the study area. The concentrations measured are minor, but the problem in this case is the large extension of land affected.

4. Conclusion

The multivariate study conducted herein offers a novel holistic methodology to assess PTE dispersion in soils in areas once used for heavy industry/mining activities and presumably subjected to a notable influence of geomorphological and climatic variables (watercourses, winds, slope, orientation and visibility), which modify the displacement of contaminants.

Our study reveals that practically the entire study area used as a paradigmatic example (a 1-km radius around a very highly polluted site) is affected by two main sources of pollution (spoil heaps and chimneys of a former Hg mining-metallurgy site), and four pollutants found by PCA: As, Hg, Sb and to a lesser extent Pb. These results were also assessed through CoDa analysis, which is the correct and consistent approach for geochemical data. In turn, HCA divided the samples into five groups. Those most linked to the spoil heaps showed a clear relationship with factors such as slope and the presence of watercourses, evidencing heap erosion. In contrast, groups most related to the chimneys showed a high correlation to winds, slope orientation, and visibility of pollution sources. Finally, the use of MPI established that those samples whose pollutant load is attributed to the spoil heaps are present in a zone of reduced size but present extremely high concentrations of pollutants. On the other hand, zones associated with the chimneys influence show lower concentrations but are larger. Furthermore, our study reveals the usefulness of the SPI to identify priority action areas in the context of regulatory standards. Overall, geomorphological factors (parametrised as slope, orientation and visibility of the pollution sources) affect contents and distribution of soil pollutants, and they should be taken into account to address comprehensive studies, together with the different sources of pollution, the geochemical behaviour of the contaminants (high mobility of As and low mobility of Hg in this case), and climatic variables (wind, rain, etc.).

All things considered, the methodology presented herein will be useful for scientists and private/public corporations wishing to assess the mobility of pollutants and to find the focal point of environmental/health risk in complex polluted sites, and will thereby allow a reduction in the time and cost of site investigation and remediation.

Declaration of Competing Interest

The authors declare that they have no known competing financial interests or personal relationships that could have appeared to influence the work reported in this paper.

Acknowledgements

C. Boente obtained a post-doctoral contract within the program PAIDI 2020 (Ref DOC_01097) co-financed by the Junta de Andalucía (Andalusian Government, Spain) and the EU. This research did not receive any specific grant from funding agencies in the public, commercial, or not-for-profit sectors. Funding for open access charge: Universidad de Huelva / CBUA.

Appendix A. Supplementary material

Supplementary data to this article can be found online at https://doi.org/10.1016/j.catena.2021.105730.

References

Aitchison, J., 1986. The statistical analysis of compositional data. J. R. Stat. Soc. 44, 139–177. https://doi.org/10.1007/978-94-009-4109-0.

Albuquerque, M.T.D., Gerassis, S., Sierra, C., Taboada, J., Martín, J.E., Antunes, I.M.H.R., Gallego, J.R., 2017. Developing a new Bayesian Risk Index for risk evaluation of soil contamination. Sci. Total Environ. 603–604, 167–177. https://doi.org/10.1016/j.scitotenv.2017.06.068.

Beucher, A., Adhikari, K., Breuning-Madsen, H., Greve, M.B., Österholm, P., Fröjdö, S., Jensen, N.H., Greve, M.H., 2017. Mapping potential acid sulfate soils in Denmark using legacy data and LiDAR-based derivatives. Geoderma 308, 363–372. https://doi.org/10.1016/j.geoderma.2016.06.001.

Boente, C., Martín-Méndez, I., Bel-Lán, A., Gallego, J.R., 2020. A novel and synergistic geostatistical approach to identify sources and cores of Potentially Toxic Elements in soils: An application in the region of Cantabria (Northern Spain). J. Geochem. Explor. 208, 106397. https://doi.org/10.1016/j.gexplo.2019.106397.

Boente, C., Albuquerque, M.T.D., Fernández-Braña, A., Gerassis, S., Sierra, C., Gallego, J. R., 2018. Combining raw and compositional data to determine the spatial patterns of Potentially Toxic Elements in soils. Sci. Total Environ. 631–632, 1117–1126. https://doi.org/10.1016/j.scitotenv.2018.03.048.

Boente, C., Matanzas, N., García-González, N., Rodríguez-Valdés, E., Gallego, J.R., 2017. Trace elements of concern affecting urban agriculture in industrialized areas: A multivariate approach. Chemosphere 183, 546–556. https://doi.org/10.1016/j.chemosphere.2017.05.129.

Bolan, N., Kunhikrishnan, A., Thangarajan, R., Kumpiene, J., Park, J., Makino, T., Kirkham, M.B., Scheckel, K., 2014. Remediation of heavy metal(loid)s contaminated soils – To mobilize or to immobilize? J. Hazard. Mater. 266, 141–166. https://doi.org/10.1016/j.jhazmat.2013.12.018.

BOPA, Boletín Oficial del Principado de Asturias, 91, April 21, 2014. (2014). Generic Reference Levels for Heavy Metals in Soils from Principality of Asturias, Spain. https://sedemovil.asturias.es/bopa/2014/04/21/2014-06617.pdf (Accessed September 2020).

Borůvka, Luboš, Vacek, Oldřich, Jehlička, Jan, 2005. Principal component analysis as a tool to indicate the origin of potentially toxic elements in soils. Geoderma 128 (3-4), 289–300. https://doi.org/10.1016/j.geoderma.2005.04.010.

Brady, J.P., Ayoko, G.A., Martens, W.N., Goonetilleke, A., 2015. Development of a hybrid pollution index for heavy metals in marine and estuarine sediments. Environ. Monit. Assess. 187, 306. https://doi.org/10.1007/s10661-015-4563-x.

Braga, Luis P.V., Braga, Jean, 2020. Mapping gold pathfinder metal ratios in Northern Nevada, USA: A compositional analysis approach. J. Geochem. Explor. 219, 106616. https://doi.org/10.1016/j.gexplo.2020.106616.

Camarero, L., 2017. Atmospheric Chemical Loadings in the High Mountain: Current Forcing and Legacy Pollution, pp. 325–341. http://dx.doi.10.1007/978-3-319-55982-7_14.

Comas-Cufí, M., Thió-Henestrosa, S., 2011. CoDaPack 2.0: a stand-alone, multi-platform compositional software. In: Egozcue, J.J., Tolosana-Delgado, R., Ortego, M.I. (Eds.) CoDaWork'11: 4th International Workshop on Compositional Data Analysis. Sant Feliu de Guíxols.

Dołęgowska, S., Michalik, A., 2019. The use of a geostatistical model supported by multivariate analysis to assess the spatial distribution of mercury in soils from historical mining areas: Karczówka Mt., Miedzianka Mt., and Rudki (south-central Poland). Environ. Monit. Assess. 191, 302. https://doi.org/10.1007/s10661-019-7368-5.

Esri Inc., 2014. ArcGIS (version 10.2.2). Software. Redlands, CA.

Facchinelli, A., Sacchi, E., Mallen, L., 2001. Multivariate statistical and GIS-based approach to identify heavy metal sources in soils. Environ. Pollut. 114 (3), 313–324. https://doi.org/10.1016/S0269-7491(00)00243-8.

Fernández, Begoña, Lara, Luis M., Menéndez-Aguado, Juan M., Ayala, Julia, García-González, Nerea, Salgado, Lorena, Colina, Arturo, Gallego, José Luis R., 2020. A multi-faceted, environmental forensic characterization of a paradigmatic brownfield polluted by hazardous waste containing Hg, As, PAHs and dioxins. Sci. Total Environ. 726, 138546. https://doi.org/10.1016/j.scitotenv.2020.138546.

Fernández, S., Cotos-Yáñez, T., Roca-Pardiñas, J., Ordóñez, C., 2018. Geographically Weighted Principal Components Analysis to assess diffuse pollution sources of soil heavy metal: Application to rough mountain areas in Northwest Spain. Geoderma 311, 120–129. https://doi.org/10.1016/j.geoderma.2016.10.012.

Florinsky, Igor V., 1998. Combined analysis of digital terrain models and remotely sensed data in landscape investigations. Prog. Phys. Geogr. Earth Environ. 22 (1), 33–60. https://doi.org/10.1177/030913339802200102.

Gallego, J.R., Esquinas, N., Rodríguez-Valdés, E., Menéndez-Aguado, J.M., Sierra, C., 2015. Comprehensive waste characterization and organic pollution co-occurrence in a Hg and As mining and metallurgy brownfield. J. Hazard. Mater. 300, 561–571. https://doi.org/10.1016/j.jhazmat.2015.07.029.

Gallini, L., Ajmone-Marsan, F., Scalenghe, R., 2018. The contamination legacy of a decommissioned iron smelter in the Italian Alps. J. Geochem. Explor. 186, 121–128. https://doi.org/10.1016/j.gexplo.2017.12.013.

Gelaro, Ronald, McCarty, Will, Suárez, Max J., Todling, Ricardo, Molod, Andrea, Takacs, Lawrence, Randles, Cynthia A., Darmenov, Anton, Bosilovich, Michael G., Reichle, Rolf, Wargan, Krzysztof, Coy, Lawrence, Cullather, Richard, Draper, Clara, Akella, Santha, Buchard, Virginie, Conaty, Austin, da Silva, Arlindo M., Gu, Wei, Kim, Gi-Kong, Koster, Randal, Lucchesi, Robert, Merkova, Dagmar, Nielsen, Jon Eric, Partyka, Gary, Pawson, Steven, Putman, William, Rienecker, Michele, Schubert, Siegfried D., Sienkiewicz, Meta, Zhao, Bin, 2017. The Modern-Era Retrospective Analysis for Research and Applications, Version 2 (MERRA-2). J. Clim. 30 (14), 5419–5454. https://doi.org/10.1175/JCLI-D-16-0758.1.

Goovaerts, P., 1999. Geostatistics in soil science: State-of-the-art and perspectives. Geoderma 89 (1-2), 1–45. https://doi.org/10.1016/S0016-7061(98)00078-0.

Hernández-Pellón, A., Nischkauer, W., Limbeck, A., Fernández-Olmo, I., 2018. Metal (loid) bioaccessibility and inhalation risk assessment: A comparison between an urban and an industrial area. Environ. Res. 165, 140–149. https://doi.org/10.1016/j.envres.2018.04.014.

Hooda, Peter S. (Ed.), 2010. Trace Elements in Soils. Wiley.

Hudson-Edwards, K., 2016. Tackling mine wastes. Science (80-.) 352 (6283), 288–290. https://doi.org/10.1126/science:aaf3354.

IBM Corp., 2016. IBM SPSS Statistics for Windows, Version 24.0. IBM Corp, Armonk, NY.

Jin, Zhao, Lv, Jianshu, 2020. Integrated receptor models and multivariate geostatistical simulation for source apportionment of potentially toxic elements in soils. CATENA 194, 104638. https://doi.org/10.1016/j.catena.2020.104638.

Kabata-Pendias, A., 2011. Trace elements in soils and plants. CRC Press. http://dx.doi.10.1201/b10158-25.

Kaiser, Henry F., 1974. An index of factorial simplicity. Psychometrika 39 (1), 31–36. https://doi.org/10.1007/BF02291575.

Khanam, Rubina, Kumar, Anjani, Nayak, A.K., Shahid, Md., Tripathi, Rahul, Vijayakumar, S., Bhaduri, Debarati, Kumar, Upendra, Mohanty, Sangita, Panneerselvam, P., Chatterjee, Dibyendu, Satapathy, B.S., Pathak, H., 2020. Metal (loid)s (As, Hg, Se, Pb and Cd) in paddy soil: Bioavailability and potential risk to human health. Sci. Total Environ. 699, 134330. https://doi.org/10.1016/j.scitotenv.2019.134330.

Lado, Luis Rodríguez, Hengl, Tomislav, Reuter, Hannes I., 2008. Heavy metals in European soils: A geostatistical analysis of the FOREGS Geochemical database. Geoderma 148 (2), 189–199. https://doi.org/10.1016/j.geoderma.2008.09.020.

Larios, Raquel, Fernández-Martínez, Rodolfo, Silva, Verónica, Loredo, Jorge, Rucandio, Isabel, 2012. Arsenic contamination and speciation in surrounding waters of three old cinnabar mines. J. Environ. Monit. 14 (2), 531–542. https://doi.org/10.1039/C1EM10684H.

Lieberman, Nir Roy, Izquierdo, Maria, Muñoz-Quirós, Carmen, Cohen, Haim, Chenery, Simon R., 2020. Geochemical signature of superhigh organic sulphur Raša coals and the mobility of toxic trace elements from combustion products and polluted soils near the Plomin coal-fired power station in Croatia. Appl. Geochemistry 114, 104472. https://doi.org/10.1016/j.apgeochem.2019.104472.

Loredo, Jorge, Luque Cabal, Carlos, Garcia Iglesias, Jesus, 1988. Conditions of formation of mercury deposits from the Cantabrian zone (Spain). Bull. Minéralogie 111 (3), 393–400. https://doi.org/10.3406/bulmi.1988.8060.

Loredo, J., Ordonez, A., Alvarez, R., 2006. Environmental impact of toxic metals and metalloids from the Muñón Cimero mercury-mining area (Asturias, Spain). J. Hazard. Mater. 136 (3), 455–467. https://doi.org/10.1016/j.jhazmat.2006.01.048.

Loska, Krzysztof, Wiechuła, Danuta, Korus, Irena, 2004. Metal contamination of farming soils affected by industry. Environ. Int. 30 (2), 159–165. https://doi.org/10.1016/S0160-4120(03)00157-0.

Martínez-Guijarro, Remedios, Paches, Maria, Romero, Inmaculada, Aguado, Daniel, 2019. Enrichment and contamination level of trace metals in the Mediterranean marine sediments of Spain. Sci. Total Environ. 693, 133566. https://doi.org/10.1016/j.scitotenv.2019.07.372.

Matanzas, N., Sierra, M.J., Afif, E., Díaz, T.E., Gallego, J.R., Millán, R., 2017. Geochemical study of a mining-metallurgy site polluted with As and Hg and the transfer of these contaminants to Equisetum sp. J. Geochem. Explor. 182, 1–9. https://doi.org/10.1016/j.gexplo.2017.08.008.

McBratney, A.B., Mendonça Santos, M.L., Minasny, B., 2003. On digital soil mapping. Geoderma 117 (1-2), 3–52. https://doi.org/10.1016/S0016-7061(03)00223-4.

McIlwaine, R., Doherty, R., Cox, S.F., Cave, M., 2017. The relationship between historical development and potentially toxic element concentrations in urban soils. Environ. Pollut. 220, 1036–1049. https://doi.org/10.1016/j.envpol.2016.11.040.

McKinley, J.M., Hron, K., Grunsky, E.C., Reimann, C., de Caritat, P., Filzmoser, P., van den Boogaart, K.G., Tolosana-Delgado, R., 2016. The single component geochemical map: Fact or fiction? J. Geochem. Explor. 162, 16–28. https://doi.org/10.1016/j.gexplo.2015.12.005.

Meeker, W.Q., Hahn, G.J., Escobar, L.A., 2017. Statistical Intervals, Wiley Series in Probability and Statistics. John Wiley & Sons, Inc., Hoboken, NJ, USA. http://dx.doi.10.1002/9781118594841.

Meteoblue., 2021. www.meteoblue.com (Accessed 1 July, 2021).

Okkenhaug, Gudny, Zhu, Yong-Guan, He, Junwen, Li, Xi, Luo, Lei, Mulder, Jan, 2012. Antimony (Sb) and Arsenic (As) in Sb Mining Impacted Paddy Soil from Xikuangshan, China: Differences in Mechanisms Controlling Soil Sequestration and Uptake in Rice. Environ. Sci. Technol. 46 (6), 3155–3162. https://doi.org/10.1021/es2022472.

Opekunova, Marina, Opekunov, Anatoly, Somov, Vsevolod, Kukushkin, Stepan, Papyan, Elza, 2020. Transformation of metals migration and biogeochemical cycling under the influence of copper mining production (the Southern Urals). CATENA 189, 104512. https://doi.org/10.1016/j.catena.2020.104512.

Paiu, Madalina, Iancu, Ovidiu Gabriel, Breaban, Iuliana Gabriela, 2017. Geochemical distribution of trace elements in an abandoned waste mine dump from Giumalau mountains, Romania. Environ. Eng. Manag. J. 16 (4), 847–857. https://doi.org/10.30638/eemj.2017.086.

Pawlowsky-Glahn, V., Egozcue, J.J., 2006. Compositional data and their analysis: an introduction. Geol. Soc. London. Spec. Publ. 264 (1), 1–10. https://doi.org/10.1144/GSL.SP.2006.264.01.01.

Petrik, A., Thiombane, M., Albanese, S., Lima, A., De Vivo, B., 2018. Source patterns of Zn, Pb, Cr and Ni potentially toxic elements (PTEs) through a compositional discrimination analysis: A case study on the Campanian topsoil data. Geoderma 331, 87–99. https://doi.org/10.1016/j.geoderma.2018.06.019.

Pobi, Krishnendu Kumar, Nayek, Sumanta, Gope, Manash, Rai, Atul Kumar, Saha, Rajnarayan, 2020. Sources evaluation, ecological and health risk assessment of potential toxic metals (PTMs) in surface soils of an industrial area. Environ. Geochem. Health. 42 (12), 4159–4180. https://doi.org/10.1007/s10653-020-00517-2.

Qiao, Jiangbo, Zhu, Yuanjun, Jia, Xiaoxu, Shao, Ming'an, Niu, Xiaoqian, Liu, Jinyue, 2020. Distributions of arsenic and other heavy metals, and health risk assessments for groundwater in the Guanzhong Plain region of China. Environ. Res. 181, 108957. https://doi.org/10.1016/j.envres.2019.108957.

Rate, A.W., 2018. Multielement geochemistry identifies the spatial pattern of soil and sediment contamination in an urban parkland, Western Australia. Sci. Total Environ. 627, 1106–1120. https://doi.org/10.1016/j.scitotenv.2018.01.332.

Reimann, C., De Caritat, P., 2005. Distinguishing between natural and anthropogenic sources for elements in the environment: regional geochemical surveys versus enrichment factors. Sci. Total Environ. 337, 91e107.

Sahoo, Prafulla Kumar, Dall'Agnol, Roberto, Salomão, Gabriel Negreiros, Junior, Jair da Silva Ferreira, Silva, Marcio Sousa, e Souza Filho, Pedro Walfir Martins, da Costa, Marcondes Lima, Angélica, Rômulo Simões, Filho, Carlos Augusto Medeiros, da Costa, Marlene Furtado, Guilherme, Luiz Roberto Guimarães, Siqueira, José Oswaldo, 2020. Regional-scale mapping for determining geochemical background values in soils of the Itacaiúnas River Basin, Brazil: The use of compositional data analysis (CoDA). Geoderma 376, 114504. https://doi.org/10.1016/j.geoderma.2020.114504.

Santos-Francés, F., Martínez-Graña, A., Zarza, C., Sánchez, A., Rojo, P., 2017. Spatial Distribution of Heavy Metals and the Environmental Quality of Soil in the Northern Plateau of Spain by Geostatistical Methods. Int. J. Environ. Res. Public Health 14, 568. https://doi.org/10.3390/ijerph14060568.

Schaefer, Kristin, Einax, Jürgen W., 2016. Source Apportionment and Geostatistics: An Outstanding Combination for Describing Metals Distribution in Soil. CLEAN - Soil, Air, Water 44 (7), 877–884. https://doi.org/10.1002/clen.v44.710.1002/clen.201400459.

Schnitzler, N., Ross, P.-S., Gloaguen, E., 2019. Using machine learning to estimate a key missing geochemical variable in mining exploration: Application of the Random Forest algorithm to multi-sensor core logging data. J. Geochem. Explor. 205, 106344. https://doi.org/10.1016/j.gexplo.2019.106344.

Sierra, C., Boado, C., Saavedra, A., Ordóñez, C., Gallego, J.R., 2014. Origin, patterns and anthropogenic accumulation of potentially toxic elements (PTEs) in surface sediments of the Avilés estuary (Asturias, northern Spain). Mar. Pollut. Bull. 86 (1-2), 530–538. https://doi.org/10.1016/j.marpolbul.2014.06.052.

Tapia, J., Murray, J., Ormachea, M., Tirado, N., Nordstrom, D.K., 2019. Origin, distribution, and geochemistry of arsenic in the Altiplano-Puna plateau of Argentina, Bolivia, Chile, and Perú. Sci. Total Environ. 678, 309–325. https://doi.org/10.1016/j.scitotenv.2019.04.084.

Teixeira, Renato Alves, de Souza, Edna Santos, de Lima, Mauricio Wilians, Dias, Yan Nunes, da Silveira Pereira, Wendel Valter, Fernandes, Antonio Rodrigues, 2019. Index of geoaccumulation and spatial distribution of potentially toxic elements in the Serra Pelada gold mine. J. Soils Sediments 19 (7), 2934–2945. https://doi.org/10.1007/s11368-019-02257-y.

Thomas, I.A., Jordan, P., Mellander, P.-E., Fenton, O., Shine, O., Ó hUallacháin, D., Creamer, R., McDonald, N.T., Dunlop, P., Murphy, P.N.C., 2016. Improving the identification of hydrologically sensitive areas using LiDAR DEMs for the delineation and mitigation of critical source areas of diffuse pollution. Sci. Total Environ. 556, 276–290. https://doi.org/10.1016/j.scitotenv.2016.02.183.

Tolosana-Delgado, Raimon, Mueller, Ute, van den Boogaart, K. Gerald, 2019. Geostatistics for compositional data: an overview. Math. Geosci. 51 (4), 485–526. https://doi.org/10.1007/s11004-018-9769-3.

Vangronsveld, J., Cunningham, S.D., 1998. Introduction to the concepts. In: Vangronsveld, J., Cunningham, S.D. (Eds.), Metal Contaminated Soils. In-Situ Inactivation and Phytorestoration, Springer-Verlag, Berlin, pp. 219–225.

Vinten, A., Sample, J., Ibiyemi, A., Abdul-Salam, Y., Stutter, M., 2017. A tool for cost-effectiveness analysis of field scale sediment-bound phosphorus mitigation measures and application to analysis of spatial and temporal targeting in the Lunan Water catchment. Scotland. Sci. Total Environ. 586, 631–641. https://doi.org/10.1016/j.scitotenv.2017.02.034.

Wang, Xutong, Dan, Zeng, Cui, Xiaoqiang, Zhang, Ruixue, Zhou, Shengquan, Wenga, Terrence, Yan, Beibei, Chen, Guanyi, Zhang, Qiangying, Zhong, Lei, 2020. Contamination, ecological and health risks of trace elements in soil of landfill and geothermal sites in Tibet. Sci. Total Environ. 715, 136639. https://doi.org/10.1016/j.scitotenv.2020.136639.

Webster, Richard, Oliver, Margaret A. (Eds.), 2007. Statistics in PracticeGeostatistics for Environmental Scientists. John Wiley & Sons, Ltd, Chichester, UK.

Woodruff, L., Cannon, W.F., Smith, D.B., Solano, F., 2015. The distribution of selected elements and minerals in soil of the conterminous United States. J. Geochem. Explor. 154, 49–60. https://doi.org/10.1016/j.gexplo.2015.01.006.

Xie, Shengyu, Yu, Guangwei, Ma, Jianli, Wang, Gang, Wang, Qichuan, You, Futian, Li, Jie, Wang, Yin, Li, Chunxing, 2020. Chemical speciation and distribution of potentially toxic elements in soilless cultivation of cucumber with sewage sludge biochar addition. Environ. Res. 191, 110188. https://doi.org/10.1016/j.envres.2020.110188.

Xie, X., Ren, T., Sun, H., 2012. Geochemical Atlas of China. Geological Publishing House, Beijing, p. 135.

Yu, H.-Y., Liu, C., Zhu, J., Li, F., Deng, D.-M., Wang, Q., Liu, C., 2016. Cadmium availability in rice paddy fields from a mining area: The effects of soil properties highlighting iron fractions and pH value. Environ. Pollut. 209, 38–45. https://doi.org/10.1016/j.envpol.2015.11.021.